

## **UC Davis**

### **UC Davis Previously Published Works**

#### **Title**

Preparation of activated carbon and silica particles from rice straw

#### **Permalink**

<https://escholarship.org/uc/item/67p8r1k8>

#### **Journal**

ACS Sustainable Chemistry and Engineering, 2(4)

#### **ISSN**

2168-0485

#### **Authors**

Hu, S

Hsieh, YL

#### **Publication Date**

2014-04-07

#### **DOI**

10.1021/sc5000539

Peer reviewed

## 1 Preparation of Activated Carbon and Silica Particles from Rice Straw

2 Sixiao Hu<sup>†</sup> and You-Lo Hsieh<sup>\*,†</sup>3 <sup>†</sup>Fiber and Polymer Science, University of California, Davis, One Shields Avenue, Davis, California 95616, United States4 **S** Supporting Information

5 **ABSTRACT:** An efficient three-step process using toluene/  
6 ethanol, NaClO<sub>2</sub>, and KOH has been successfully devised to  
7 isolate pure cellulose from rice straw while generating two  
8 filtrates as activated carbon and silica precursors. The NaClO<sub>2</sub>  
9 dissolution filtrate contains oxidized lignin and hemicellulose  
10 as carbon precursors as well as sodium carbonates as activating  
11 agents for direct carbonization (800 °C) into highly porous  
12 (0.90 cm<sup>3</sup>/g), high specific surface area (997 m<sup>2</sup>/g), activated  
13 carbon particles (100–500 nm). The KOH dissolution filtrate  
14 contains mainly potassium silicate that could be precipitated  
15 by dilute acidified poly(ethylene oxide) and calcinated (500 °C)  
16 to pure, uniformly sized (100–120 nm), nonporous silica  
17 nanospheres. Deriving these additional activated carbon and silica  
18 particles along with nanocellulose creates advance materials  
19 while fully utilizing all major components in rice straw, the highest quantity agricultural crop byproduct in the world.

18 **KEYWORDS:** Activated carbon, Porous, Monodispersed silica, Green chemistry, Rice straw utilization,



## 19 ■ INTRODUCTION

20 Lignocellulosic biomass, such as agricultural crop residues,  
21 forestry byproducts, and municipal waste, is a rich source of  
22 renewable energy and materials. Lignocellulosic materials have  
23 been converted to biofuel such as ethanol,<sup>1–3</sup> hydrogen, and  
24 other combustible gases,<sup>4,5</sup> as well as nanocellulose,<sup>3–5</sup>  
25 carbon,<sup>2,5</sup> and silicon-based<sup>6,7</sup> materials. Cellulose nanocrystals  
26 and nanofibrils have been isolated from various major  
27 agricultural residuals including rice straw,<sup>6</sup> wheat straw, and  
28 soy hulls.<sup>7</sup> Direct thermal processing of various biomass has  
29 also generated charcoals,<sup>4</sup> activated carbon,<sup>8</sup> and silicon-based  
30 advanced materials including mesoporous silica<sup>9</sup> as well as  
31 silicon carbide and nitride.<sup>10</sup> Simultaneous derivation of parallel  
32 products from specific biomass for full utilization has not been  
33 given much attention.

34 Rice straw represents the largest agricultural byproduct  
35 around the world. Rice is the largest cereal crop and the highest  
36 valued agricultural commodity (\$187 billion in 2011) in the  
37 world.<sup>11</sup> Although third in quantity (723 million MT in 2011)  
38 behind sugar cane and maize, rice production generates the  
39 highest quantity of byproduct as rice straw accounts from 1 to  
40 1.5 kg per kg of rice grain harvested.<sup>12</sup> Direct use has presented  
41 some shortcomings as rice straw is a marginal feed compared  
42 with other cereal straw and causes severe furnace fouling and  
43 ash production when burned to produce steam.

44 Other utilization of rice straw has mainly involved single  
45 product development by converting certain components while  
46 removing others employing biochemical, chemical, and/or  
47 thermal processes. Ethanol production was improved by  
48 enzymatic saccharification of cellulose and hemicellulose,<sup>13</sup>  
49 while hydrogen-rich gas production was made efficient via  
50 microwave-assisted pyrolysis of rice straw.<sup>14</sup> Long, highly  
51 crystalline, cellulose fibers have been extracted from rice

52 straw via alkali and enzymatic methods.<sup>15</sup> Activated carbons 52  
53 were prepared from rice straw by KOH activation and 53  
54 carbonization at 800–900 °C<sup>16,17</sup> or preoxidation at 200 °C 54  
55 and (NH<sub>4</sub>)<sub>2</sub>HPO<sub>4</sub> activation at 700 °C<sup>18</sup> to reach 1900 and 55  
56 1150 m<sup>2</sup>/g specific surface areas, respectively, comparable to 56  
57 commercially available activated carbon products. Silica nano- 57  
58 spheres were prepared from alkali dissolution of burned straw 58  
59 ashes and then acid precipitation<sup>19</sup> to better control nano- 59  
60 particle sizes from 16 to 100 nm.<sup>20</sup> Uniform nanodisks were 60  
61 also prepared by sulfuric acid precipitation of dissolved silica 61  
62 from rice straw ashes, followed by freeze-drying.<sup>21</sup> Silicon 62  
63 carbide and nitride nanorods were fabricated by direct pyrolysis 63  
64 of rice straw under nitrogen from 1400 to 1800 °C.<sup>22</sup>

65 The significant lignocellulosics, that is, 32–47% cellulose, 65  
66 19–27% hemicellulose, and 5–24% lignin, as well as 7–20% 66  
67 silica and trivial amount of waxes and minerals in rice 67  
68 straw<sup>20,23–27</sup> present opportunities for simultaneous develop- 68  
69 ment of multiple products. We have developed a simple 69  
70 approach to isolate cellulose, lignin/hemicelluloses, and silica 70  
71 components in rice straw with minimal chemical and energy 71  
72 input.<sup>6</sup> Pure cellulose was extracted from rice straw via an 72  
73 efficient NaClO<sub>2</sub>–KOH process with at least 36% yield, where 73  
74 dewaxing in 2:1 v/v toluene/ethanol extraction was followed by 74  
75 lignin removal via acidified NaClO<sub>2</sub> and then hemicellulose and 75  
76 silica isolation by KOH. Cellulose nanocrystals and nanofibrils 76  
77 have been derived from pure rice celluloses via sulfuric acid 77  
78 hydrolysis<sup>6,28</sup> and 2,2,6,6-tetramethylpiperidine-1-oxyl 78  
79 (TEMPO)-mediated oxidation,<sup>28</sup> respectively, and then 79  
80 assembled into fibrous and porous matrixes.

Received: October 9, 2013

Revised: February 11, 2014

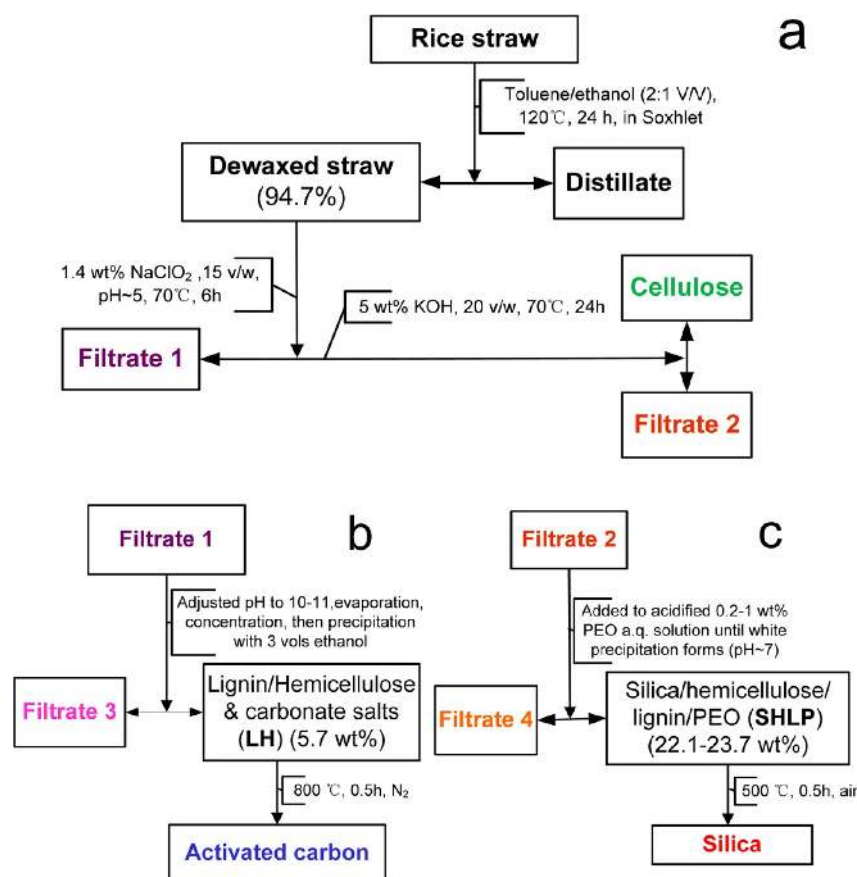


**Figure 1.** Scheme for (a) isolation of celluloses, lignin-rich filtrate 1, and silica-rich filtrate 2 from rice straw; (b) activated carbon from filtrate 1; and (c) silica from filtrate 2.

81 The goal of this work was to develop additional advanced  
 82 materials from the as-derived extracts of two dissolution  
 83 streams in isolating pure cellulose toward utilization of all  
 84 major rice straw components, that is, lignin, hemicelluloses, and  
 85 silica.  $\text{NaClO}_2$  and KOH were used as the former is a strong  
 86 oxidant that could break the strong bonding among the  
 87 lignocellulosics, and the latter could dissolve silica in rice straw.  
 88 The  $\text{NaClO}_2$  dissolution stream from the dewaxed rice straw  
 89 contains oxidation products of lignin and hemicellulose as well  
 90 as sodium byproducts. As lignin and hemicelluloses were  
 91 intrinsically bound to each other and thus very difficult to be  
 92 completely separated without sacrificing one or another to  
 93 soluble fragments, it is advantageous and economic to use this  
 94 lignin/hemicelluloses mixture together as a carbon source,  
 95 while sodium salts already present could serve as the activating  
 96 agents to produce porous structures without needing further  
 97 addition of chemicals. The KOH dissolution stream from  
 98  $\text{NaClO}_2$ -treated rice straw should contain mainly potassium  
 99 silicate, which may serve as a precursor to silica. These  
 100 precursors in both streams would be recovered by precipitation  
 101 using ethanol for lignin/hemicelluloses carbon precursors and  
 102 acidified poly(ethylene oxide) for the silica precursors. These  
 103 two precursors could be thermally converted to carbon and  
 104 silica products via a single-step pyrolysis and calcinations at 800  
 105 and 500 °C, respectively.

## 106 ■ EXPERIMENTAL DETAILS

107 **Chemicals.** Rice straw (Calrose variety) used in this study was  
 108 from the 2009 harvest in the Sacramento valley in northern California.  
 109 Toluene ( $\text{C}_6\text{H}_5\text{CH}_3$ , ACS grade, Fisher Scientific), ethanol

( $\text{CH}_3\text{CH}_2\text{OH}$ , anhydrous, histological grade, Fisher Scientific), 110  
 sodium chlorite ( $\text{NaClO}_2$ , 80%, Fluka), glacial acetic acid 111  
 ( $\text{CH}_3\text{COOH}$ , 99.7%, ACS GR, EMD), poly(ethylene oxide) (PEO) 112  
 ( $M_w = 600$  kDa, Sigma-Aldrich), and potassium hydroxide (KOH, 113  
 85%, EM Science) for fractionating rice straw components were used  
 114 as received. Water used was purified by a Milli-Qplus water  
 115 purification system (Millipore Corporate, Billerica, MA). All  
 116 concentration and yield percentage values were based on weight  
 117 unless otherwise specified. 118

**Preparation of Activated Carbon and Silica Particles from**  
**Rice Straw.** Fractional extraction of lignin/hemicelluloses and silica  
 120 from rice straw was first performed by the  $\text{NaClO}_2$  treatment as shown  
 121 in Figure 1. Rice straw was washed thoroughly with water to rid of dirt,  
 122 dried, and then milled (Thomas-Wiley Laboratory Mill model 4,  
 123 Thomas Scientific, U.S.A.) to pass through mesh 60. Rice straw  
 124 powders were Soxhlet extracted with 2:1 toluene/ethanol (v/v) at 55  
 125 °C for 24 h to remove all lipophilic and hydrophilic nonstructural  
 126 components (Figure 1). The dewaxed rice straw powder was placed in  
 127 1.4 wt %  $\text{NaClO}_2$  under acidic condition (pH ~5 adjusted by 10%  
 128 acetic acid) at a 15 mL/g liquid-to-solid ratio at 70 °C for 6 h and  
 129 filtered to yield holocellulose/silica and filtrate 1.  $\alpha$ -Cellulose was  
 130 isolated from holocellulose by extracting with 5 wt % KOH at a  
 131 20 mL/g liquid-to-solid ratio at 70 °C for 24 h to give pure cellulose and  
 132 dissolved silica and hemicelluloses in filtrate 2. Both filtrate 1 and 2  
 133 were then concentrated by heating at 90 °C to half their volumes. The  
 134 remaining filtrates 4 and 5 contained mostly water with very little  
 135 solutes. Ethanol in filtrate 4 may be recovered by distillation. 136

**Preparation of Activated Carbon.** Ethanol was added to the  
 137 concentrated filtrate 1 at 3 times its volume to precipitate alkali-soluble  
 138 lignin together with some hemicelluloses (LH). The LH powders were  
 139 dried in oven at 60 °C for 12 h, placed in a quartz tube (2 cm inner  
 140 diameter), and then pyrolyzed in a furnace (Mini-Mite, Lindberg/  
 141 Blue) at 10 °C/min to 105 °C and held for 0.5 h. Then the LH 142

143 powders were heated to 800 °C and held for up to 0.5 h, all under  
144 flowing N<sub>2</sub> at 100 mL/min. Finally, they were cooled to ambient  
145 temperature in 12 h. The particles were washed with 5% HCl and  
146 water to remove residual salts and other small hydrocarbon impurities  
147 and then dried at 105 °C for 0.5 h to yield activated carbon (AC).

148 **Preparation of Silica Particles.** Acidified PEO solutions at 0.2%,  
149 0.35%, 0.5%, and 1% were prepared by dissolving 0.04, 0.07, 0.1, and  
150 0.2 g of PEO, respectively, in 20 g of 2% HCl and stirred for 6 h.  
151 Concentrated filtrate 2 was added slowly to each acidified PEO  
152 aqueous solution to form a milky white mixture and centrifuged  
153 (Centrifuge 5804R, Eppendorf) at 5000 rpm for 15 min. The  
154 precipitate was then washed with water thoroughly and dried in a  
155 desiccator as silica and lignin/hemicelluloses/PEO (SHLP). The dried  
156 SHLP powder was placed in a quartz tube (2 cm inner diameter) and  
157 calcinated under flowing air (100 mL/min) in a furnace (Mini-Mite,  
158 Lindberg/Blue). The sample was heated at 10 °C/min to 105 °C and  
159 then 500 °C; the sample was held for 0.5 h at each temperature. The  
160 obtained silica after calcination was cooled under flowing air (100 mL/  
161 min) to room temperature in 12 h. Filtrate 4, SHLP, and silica were  
162 referred to those obtained at 0.35% PEO unless stated otherwise.

163 **Analytical Methods.** The yields were calculated by the percentage  
164 of extract or product mass over the original rice straw mass, both 0.1  
165 mg accuracy (BP 300S, Satorius). The aqueous filtrates from the  
166 extraction process were examined by ultraviolet–visible spectroscopy  
167 (UV–vis) (Evolution 600, Thermo Scientific). UV samples were  
168 placed in polystyrene cuvettes with a 1 cm path length. The chemical  
169 composition and structure of LH, AC, SHLP, and silica were analyzed  
170 by Fourier transform infrared spectroscopy (FTIR) (Nicolet 6700,  
171 Thermo Scientific). All FTIR spectra were collected from samples  
172 dried at 60 °C for 12 h and pressed with anhydrous KBr powders into  
173 pellets. The elemental analysis of LH, AC, SHLP, and silica were  
174 carried out by energy-dispersive X-ray spectroscopy (EDX) adjunct to  
175 a scanning electron microscope (SEM) (FEI-XL 30, FEI). All samples  
176 are stored in oven at 60 °C for 24 h before EDX measurements.

177 The morphology and structure of LH and SHLP as well as their  
178 pyrolyzed products AC and silica were observed by SEM (FEI-XL 30,  
179 FEI). The SEM samples were sputter coated with gold for 2 min and  
180 then observed under a working voltage of 5 kV. The structures of AC  
181 and silica particles were also examined by transmission electron  
182 microscopy (TEM) (JEOL 3000, JEOL). TEM samples were prepared  
183 by dispersing a small amount of AC and silica particles in water (~0.01  
184 g/L) and sonicated (2510, Branson) for 60 min first, and then a drop  
185 of the sonicated suspension was placed onto a carbon grid and dried in  
186 air.

187 The thermal properties of LH and SHLP were analyzed by  
188 differential scanning calorimetry (DSC) (DSC-60, Shimadzu) and  
189 thermogravimetric analysis (TGA) (TGA-50, Shimadzu). DSC  
190 samples were tightly packed in aluminum cells with press-sealed lids,  
191 while TGA samples were placed in a platinum pan. LH samples were  
192 heated to 60 °C and held for 2 h, then heated to 105 °C and held for  
193 0.5 h, and finally heated to 550 and 800 °C for DSC and TGA,  
194 respectively, and held for 0.5 h under 50 mL/min nitrogen flow. SHLP  
195 samples were heated to 105 °C and held for 0.5 h and then heated to  
196 500 °C and held for 0.5 h under a 50 mL/min air flow.

197 For surface area and pore characteristics, LH, AC, SHLP, and silica  
198 were dried in oven at 50 °C for 48 h and then measured at 77 K by a  
199 nitrogen adsorption–desorption analyzer (ASAP 2020, Micrometrics).  
200 The surface area was calculated from the isotherm using the  
201 Brunauer–Emmett–Teller (BET) equation in the linear region  
202 where relative pressure  $P/P_0$  ranged from 0.05 to 0.1. The mesopore  
203 surface areas of LH, AC, SHLP, and silica were derived from the  
204 adsorption branch, whereas pore- and neck-size distributions were  
205 derived from both adsorption and desorption branches of the isotherm  
206 using the Barret–Joyner–Halenda (BJH) method. The micropore  
207 surface area and pore hydraulic diameter distribution (0.7–1.6 nm) of  
208 AC were derived from the  $t$ -plot using the Mikhail, Brunauer, and  
209 Bodor MP method<sup>29</sup> and the Harkins and Jura equation.<sup>30</sup> Micropore  
210 volume ( $V_{mp}$ ) was derived from the tangent line of a contiguous range  
211 of  $t$ -plots using the surface area of the filled pores via eq 1,

$$V_{mp} = \frac{(S_n - S_{n+1}) \times (t_n + t_{n-1})}{2} \times 15.47 \quad (1) \quad 212$$

where  $S_n$  and  $t_n$  are the surface area derived from the slope of tangent 213  
and the thickness of absorbed layer at the  $n$  point in the  $t$ -plot, 214  
respectively, and 15.47 was the constant of converting the gas volume 215  
to liquid volume at STP. 216

## 217 ■ RESULTS AND DISCUSSION

**Yields and Efficiency of Sodium Chlorite Isolation.** The 218  
NaClO<sub>2</sub>–KOH process for isolating rice straw components 219  
involved three steps, yielding pure cellulose as well as filtrates 1 220  
and 2 (Figure 1a). The washed and dried rice straw was 221  
refluxed in a 2:1 toluene/ethanol (v/v) ratio at 55 °C for 24 h 222  
to yield 94.7% dewaxed rice straw and a green-yellow distillate 223  
containing surface oils, pigments, and possibly organic soluble 224  
lignin. The dewaxed rice straw was then treated by 1.4% 225  
NaClO<sub>2</sub> at pH 5 adjusted by acetic acid at 70 °C for 6 h and 226  
then 5% KOH at 70 °C for 24 h to obtain pure cellulose as well 227  
as the NaClO<sub>2</sub> and alkaline dissolution streams, that is, filtrates 228  
1 and 2, respectively. Adding ethanol to filtrate 1 under the 229  
basic condition precipitated the dissolved lignin/hemicelluloses 230  
(LH) at 5.7% of the original rice straw mass (Figure 1b). 231  
Adding the basic filtrate 2 to the dilute acidified PEO 232  
precipitated silica along with remaining lignin/hemicellulose 233  
(SHLP) at similar yields of 22.1–23.7%, increasing to 0.2–1% 234  
PEO concentrations (Figure 1c). At 0.35% PEO, the silica/ 235  
hemicelluloses/lignin (SHL) yield was 20.7%, assuming all 236  
PEO precipitated. 237

**Chemical Structures of Extracts and Final Products.** 238  
NaClO<sub>2</sub> and KOH treatments yielded respective filtrates 1 and 239  
2, which were precipitated as precursors to be subsequently 240  
converted to AC and silica particles, respectively. The 241  
compositions and structures of both filtrates, their precipitates, 242  
and final products were examined by UV–vis, FTIR, and 243  
elemental analysis to determine their compositions and to 244  
assess the isolation process. 245

**UV–Vis Spectra of the Filtrates.** The UV–vis spectrum 246  
of filtrate 1 exhibited strong broad absorbance below 300 nm 247  
(Figure 2), ascribing to partially oxidized and/or decomposed 248  
lignin from NaClO<sub>2</sub>, possibly a poly(lignol) dehydrogenative 249  
copolymer of sinapyl alcohol, coniferyl alcohol, p-coumaryl 250  
alcohol, and hydroxycinnamic acid esters.<sup>31,32</sup> Filtrate 2 showed 251  
reduced yet clear UV absorbance below 300 nm, indicating the 252

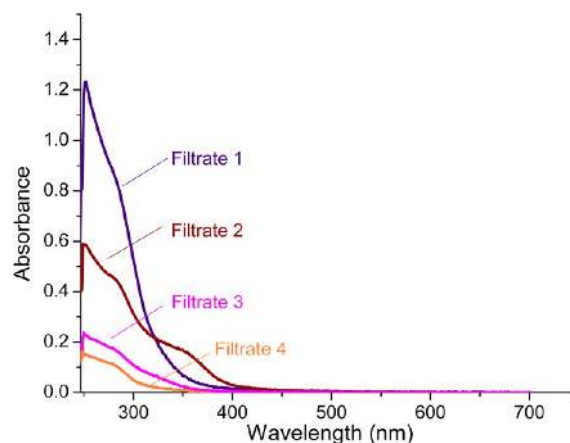


**Figure 2.** UV–vis spectra of filtrates from rice straw isolation shown in Figure 1.

253 presence of some alkaline-soluble lignin and incomplete lignin  
 254 removal in the previous  $\text{NaClO}_2$  step. The broad absorption  
 255 peak in the 360 nm region of the filtrate 2 spectra is consistent  
 256 with the expected alkaline-soluble lignin, possibly various lignin  
 257 derivatives of *o,p*-dihydroxystilbenes,  $\alpha$ -carbonyl phenolics,  
 258 esters of *p*-coumaric, and ferulic acids,<sup>33</sup> as well as charge-  
 259 transfer complexes from the carbonyl and carboxyl-conjugated  
 260 heteroaromatic compounds.<sup>34</sup> Filtrate 3 showed very little  
 261 absorbance below 300 nm, indicating effective precipitation of  
 262 lignin in LH by ethanol. Filtrate 4 also exhibited reduced peak  
 263 intensity below 300 nm, showing the presence of a small  
 264 amount of alkaline-soluble lignin in this final filtrate. The UV-  
 265 vis spectrum suggested that most lignin in rice straw was  
 266 extracted by  $\text{NaClO}_2$  dissolution in filtrate 1 and recovered by  
 267 ethanol precipitation in LH, while some lignin present in the  
 268 alkaline filtrate 2 was mostly precipitated by PEO in SHLP,  
 269 leaving yet a small residual lignin in filtrate 4. Therefore, lignin  
 270 in rice straw was recovered by precipitation mainly in LH from  
 271 filtrate 1 and partially in SHLP from filtrate 2, with a residual  
 272 amount in the final filtrate 4.

273 **FTIR Spectra of Precipitates and Final Products.** The  
 274 FTIR spectrum of the LH precipitate from filtrate 1 showed  
 275 major lignin characteristic peaks, including those between 1600  
 276 and  $1000\text{ cm}^{-1}$  from partially oxidized phenylpropanoids and  
 277 multiple hydroxyl peaks (Figure 3). Lignin was evident by the

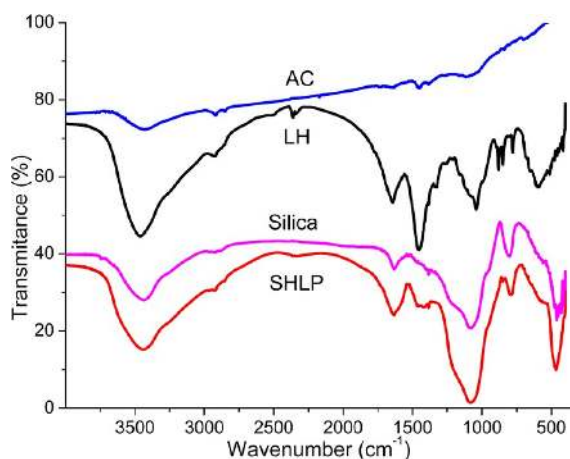


Figure 3. FTIR spectrum of LH, AC, SHLP, and silica.

278 strong  $1450$  and  $1040\text{ cm}^{-1}$  peaks associated with aromatic  
 279  $\text{C}=\text{C}$  stretching and aromatic  $=\text{C}-\text{H}$  in-plane bending,  
 280 respectively. The prominent peak at  $3459\text{ cm}^{-1}$  and two minor  
 281 peaks at  $2930$  and  $2835\text{ cm}^{-1}$  were attributed to OH stretching  
 282 in the respective hydrogen-bonded and free hydroxyls, whereas  
 283 the ones at  $1090\text{ cm}^{-1}$  were from  $\text{C}-\text{O}$  deformation in the  
 284 aliphatic hydroxyl and ether groups. The broad band at  $1630$   
 285  $\text{cm}^{-1}$  could be from moisture peaks overlapped with various  
 286  $\text{C}=\text{O}$  stretching,  $\text{C}=\text{C}$  stretching in phenylpropanoid side  
 287 chains, and aromatic skeleton vibration. Therefore, LH  
 288 precipitated from filtrate 1 consisted mainly of oxidized lignin  
 289 from reaction with the strongly oxidative  $\text{NaClO}_2$ .

290 SHLP precipitated from filtrate 2 with diluted PEO showed  
 291 characteristic peaks of silica, lignin, hemicelluloses, and PEO  
 292 (Figure 3). Silica was clearly evident by the prominent  $\text{Si}-\text{O}-$   
 293  $\text{Si}$  asymmetric and symmetric stretching peaks at  $1090$  and  $460$   
 294  $\text{cm}^{-1}$ , respectively, as well as a  $\text{Si}-\text{O}$  deformation peak at  $795$   
 295  $\text{cm}^{-1}$ . The presence of lignin was evident by the benzene  $\text{C}=\text{C}$   
 296 stretching peak at  $1460\text{ cm}^{-1}$ . However, the peak intensity

decreased greatly compared to that of LH, suggesting the  
 reduced lignin composition in SHLP. The broad shoulder at  
 $1205\text{ cm}^{-1}$  was ascribed to the various  $\text{C}-\text{O}-\text{C}$  stretching from  
 hemicelluloses and PEO. The broad shoulder at  $1640\text{ cm}^{-1}$  was  
 from moisture overlapping with  $\text{C}=\text{C}$  stretching and various  
 esters and ketone structures, such as  $\beta$  ketone ester,  $\alpha-\beta$   
 unsaturated ketone, and  $\beta$  diketone (enol form) in hemi-  
 celluloses. The broad  $3430\text{ cm}^{-1}$  peak as well as minor peaks at  
 $2930$  and  $2835\text{ cm}^{-1}$  were ascribed to hydroxyls from moisture,  
 lignin/hemicelluloses, and silica surfaces.

The pyrolytic product of LH from heating at  $800\text{ }^\circ\text{C}$  showed  
 little characteristic FTIR peaks of either lignin or hemicelluloses  
 as expected. The broad OH stretching peak around  $3440\text{ cm}^{-1}$   
 greatly decreased in intensity compared to LH, clearly showing  
 the loss of hydroxyls and is consistent with transformation of  
 hydrophilic lignin/hemicelluloses to hydrophobic carbon. The  
 only two small peaks at  $1454$  and  $1380\text{ cm}^{-1}$  were ascribed to  
 aliphatic  $\text{C}-\text{H}$  bending. Thus, the FTIR of pyrolyzed LH is  
 consistent with conversion to carbon with few lignin and  
 hemicelluloses features.

The FTIR spectrum of SHLP calcinated at  $500\text{ }^\circ\text{C}$  showed  
 only silica characteristic peaks, that is,  $\text{Si}-\text{O}-\text{Si}$  asymmetric  
 and symmetric stretching at  $1080$  and  $460\text{ cm}^{-1}$ , respectively,  
 and  $\text{Si}-\text{O}$  deformation at  $780\text{ cm}^{-1}$ , as well as the broad  
 hydroxyl stretching peaks at  $3440$  and  $1630\text{ cm}^{-1}$ , indicating  
 absorbed moisture or the hydrophilic nature of silica. None of  
 the lignin, hemicelluloses, and PEO characteristic peaks was  
 observed, confirming their removal upon calcination.

UV-vis results clearly showed that lignin-rich LH and silica/  
 hemicelluloses-rich SHLP were successfully isolated in filtrates  
 1 and 2, respectively, while FTIR confirmed that the isolated  
 lignin in LH and hemicelluloses in SHLP were oxidized and  
 degraded by the oxidative  $\text{NaClO}_2$  and then thermally  
 converted to carbon and silica, respectively.

**Elemental Analysis of Extracts.** The elemental compo-  
 sitions by EDX show LH to consist of 38.0% C, 42.8% O,  
 18.6% Na, and 0.6% Si (Table 1). The high Na and O contents

Table 1. Elemental Compositions (wt%) of Crude LH and SHLP and Their Respective Pyrolyzed Products: AC ( $800\text{ }^\circ\text{C}$ , 30 min) and Silica ( $500\text{ }^\circ\text{C}$ , 0.5 h)

	C	O	Si	Na
LH	38.0	42.8	0.6	18.6
AC	81.7	15.8	2.5	0
SHLP	16.6	51.7	29.7	0
silica	0	53.0	47.0	0

suggested LH contained oxy-salts of sodium, possibly sodium  
 carbonates, oxidative products of lignin/hemicelluloses, and  
 acetic acid in the  $\text{NaClO}_2$  step. The continuous evolution of  
 odorless bubbles when adding crude LH powder into dilute  
 aqueous HCl indicated gaseous products and was consistent  
 with the presence of carbonate salts in crude LH. To further  
 investigate the compositions of inorganic salts, LH was  
 calcinated at  $500\text{ }^\circ\text{C}$  for 6 h. The yellow color of LH turned  
 to a white color after calcination (Figure S1, Supporting  
 Information) and was shown by EDX to have the elemental  
 composition of  $\text{Na}_2\text{CO}_3$  (Figure S1, Supporting Information),  
 confirming the presence of sodium carbonates in crude LH. As  
 LH was precipitated from aqueous solution, sodium carbonate  
 should exist in the form of monohydrate after drying at  $60\text{ }^\circ\text{C}$ .  
 Under this assumption, monohydrate sodium carbonate

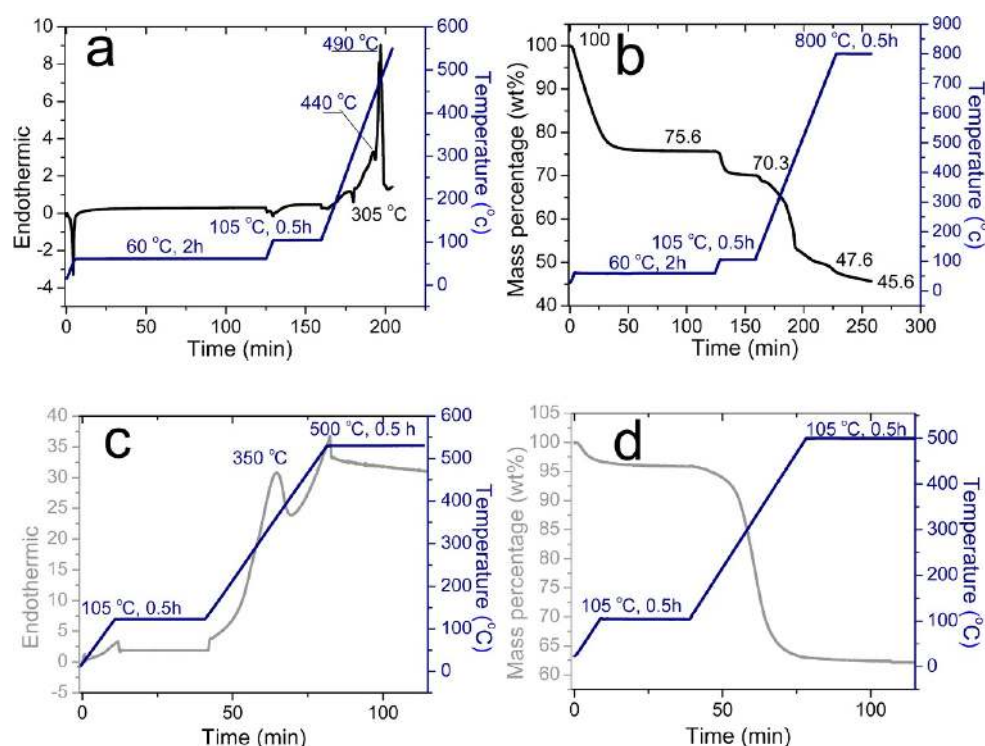


**Figure 4.** Thermal characteristics of crude LH (a,b) and SHLP (c,d): (a,c) DSC and (b,d) TGA thermographs.

349 content in the crude LH precipitate would be 50.1%, leaving  
 350 49.9% to be lignin and hemicelluloses (LH). Such a unique  
 351 composition allowed LH to be directly pyrolyzed into AC,  
 352 without the need to add additional activating chemicals, making  
 353 this pathway superior than previously reported ap-  
 354 proaches.<sup>16–18</sup> SHLP consisted of 16.6% C, 51.7% O, and  
 355 29.7% Si, showing its elemental compositions to be mainly  
 356 silica (64%) and lignin/hemicelluloses/PEO (36%). This three-  
 357 step toluene/ethanol, NaClO<sub>2</sub>, and KOH isolation process  
 358 isolated 5.3% waxes and organic extracts, 36% highly pure  
 359 cellulose,<sup>3</sup> 2.8% LH, and 20.7% SHL, or 65% of precursors,  
 360 leaving about 35% rice straw components as soluble from  
 361 NaClO<sub>2</sub> oxidation and KOH dissolution in the remaining  
 362 filtrates.

363 The chars pyrolyzed from LH after dilute HCl washing  
 364 consisted of 81.7% C, 15.8% O, and 2.5% Si, confirming  
 365 substantial carbon with little silica impurities. After calcinating  
 366 SHLP at 500 °C for 0.5 h, only 47% Si and 53% O were  
 367 detected, while no carbon was present. This mass percentage is  
 368 equivalent to a 1:2 Si/O atomic ratio or that of pure silica.

369 **Thermal Properties of Extracts.** The thermograms of LH  
 370 showed a very sharp exothermic peak at 60 °C and a small  
 371 exotherm around 105 °C (Figure 4a) with respective 24.4% and  
 372 5.3% mass losses (Figure 4b), reflecting the transition from  
 373 sodium carbonate decahydrate to monohydrate as well as  
 374 moisture loss from lignin and hemicelluloses. The endotherm at  
 375 300 °C is attributed to the decomposition of hemicelluloses,  
 376 while two exotherms at 430 and 475 °C were likely from  
 377 decomposition and further charring of lignin, corresponding to  
 378 the major 19.2% mass loss, that is, from 70.7% at 105 °C to  
 379 51.5% at 550 °C. The solid mass was lowered to 47.6% when  
 380 heated to 800 °C initially and slightly lowered to 45.6% when  
 381 held for additional 30 min.

The thermal analysis further supported the compositions  
 derived from EDX that the crude LH at ambient temperature  
 was a mixture of sodium carbonate monohydrate and  
 decahydrate as well as lignin/hemicelluloses. Assuming the  
 mass loss at 105 °C is solely caused by the transformation of  
 sodium carbonate monohydrate to the anhydrous form, the  
 weight percentages of sodium carbonate monohydrate and Na  
 in crude LH were estimated to be 48.3% and 17.9%,  
 respectively (eqs 1 and 2), very close to the 50.1% estimated  
 from EDX elemental analysis. These values are slightly higher  
 than the atomic compositions due to the missing hydrogen in  
 the EDX. The composition of crude LH precipitate at 105 °C  
 would thus be estimated to be 44.4% anhydrous sodium  
 carbonate and 55.6% lignin/hemicelluloses (eq 3). Therefore,  
 the final pyrolyzed product could be a mixture of lignin char  
 and various forms of sodium, sodium carbonate, sodium oxide,  
 and elementary sodium, all of the latter removed in the wash  
 to obtain 1.3% activated carbon (AC) from the starting rice  
 straw.

SHLP showed an endothermic shoulder below 105 °C  
 (Figure 4c) accompanied by a slight 4% mass loss from  
 moisture (Figure 4d). A broad exothermic peak centered at 350  
 °C was observed along with a significant 33% mass loss, that is,  
 from 96% at 105 °C to 63% at 500 °C, due to thermal  
 decomposition of hemicelluloses/lignin/PEO. This quantity  
 was consistent with the 64% silica from the EDX analysis.  
 When held at 500 °C for 0.5 h, the DSC thermograph baseline  
 shifted endothermically, while the solid mass slightly decreased  
 from 63% to 61.5%, indicating further combustion of the  
 residual carbon char, obtaining 14% pure silica from the starting  
 rice straw.

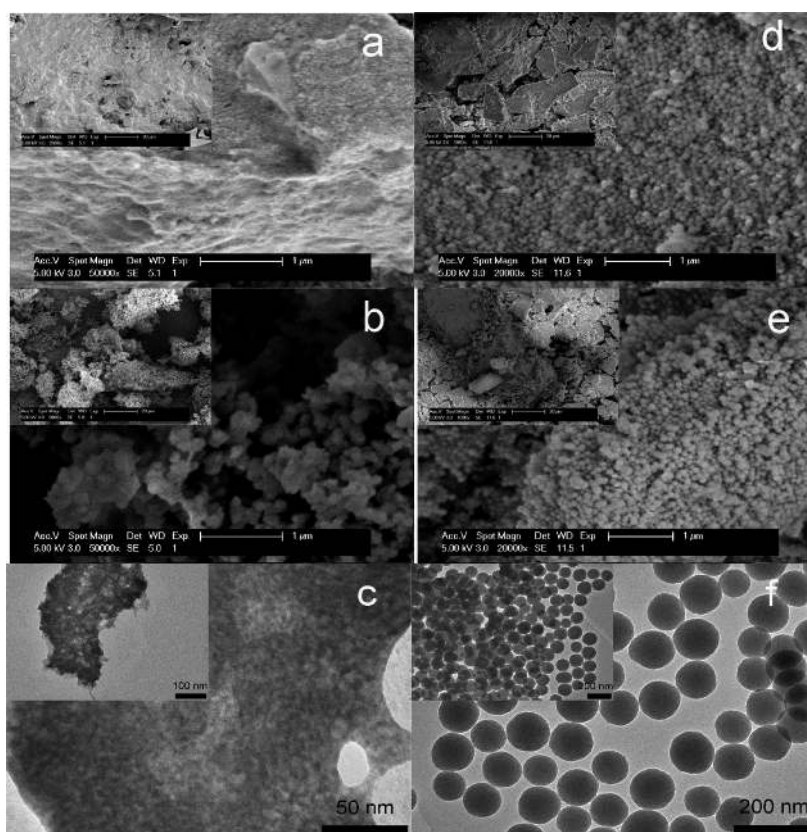


**Figure 5.** SEM (a,b,d,e) and TEM (c,f) of (a) LH, (b,c) AC, (d) SHLP, and (e,f) silica. Insets in SEM: scale bar = 20  $\mu\text{m}$ .

$$\text{Na}_2\text{CO}_3 \cdot \text{H}_2\text{O}_{(\text{at } 60^\circ\text{C})} (\text{wt}\%) = \frac{\text{Mass loss from Na}_2\text{CO}_3 \cdot \text{H}_2\text{O to Na}_2\text{CO}_3 (\text{wt}\%) \times \text{Molar mass of Na}_2\text{CO}_3 \cdot \text{H}_2\text{O}}{\text{Molar mass of H}_2\text{O} \times \text{Mass percentage of solid residue}_{(\text{at } 60^\circ\text{C})}} = \frac{5.3 \text{ wt}\% \times 124}{18 \times 0.756} = 48.3 (\text{wt}\%) \quad (1)$$

$$\text{Na}_{(\text{at } 60^\circ\text{C})} (\text{wt}\%) = \text{Na}_2\text{CO}_3 \cdot \text{H}_2\text{O}_{(\text{at } 60^\circ\text{C})} (\text{wt}\%) \times \frac{\text{Molar mass of Na} \times 2}{\text{Molar mass of Na}_2\text{CO}_3 \cdot \text{H}_2\text{O}} = 48.3 \times \frac{46}{124} = 17.9 (\text{wt}\%) \quad (2)$$

$$\text{Na}_2\text{CO}_3_{(\text{at } 60^\circ\text{C})} (\text{wt}\%) = \text{Na}_2\text{CO}_3 \cdot \text{H}_2\text{O}_{(\text{at } 60^\circ\text{C})} (\text{wt}\%) \times \frac{\text{Molar mass of Na}_2\text{CO}_3}{\text{Molar mass of Na}_2\text{CO}_3 \cdot \text{H}_2\text{O}} = 48.3 \times \frac{106}{124} = 41.3 (\text{wt}\%) \quad (3)$$

$$\text{Na}_2\text{CO}_3_{(\text{at } 60^\circ\text{C})} (\text{wt}\%) = \frac{\text{Na}_2\text{CO}_3_{(\text{at } 60^\circ\text{C})} (\text{wt}\%)}{\text{Na}_2\text{CO}_3_{(\text{at } 60^\circ\text{C})} (\text{wt}\%) + (100 - \text{Na}_2\text{CO}_3 \cdot \text{H}_2\text{O}_{(\text{at } 60^\circ\text{C})} (\text{wt}\%))} \times 100 = \frac{41.3}{41.3 + 100 - 48.3} \times 100 = 44.4 (\text{wt}\%) \quad (4)$$

On the basis of the TGA analysis, the LH component contained 51% sodium salt or about 2.8% yield of lignin/hemicelluloses from  $\text{NaClO}_2$  dissolution of rice straw (e.g., filtrate 1). SHLP consisted of 61.5% silica, 29.3% lignin/hemicelluloses, and 9.2% PEO or 14% silica and 6.7% lignin/hemicelluloses yields from the KOH dissolution stream (e.g., filtrate 2). From these and our prior report on cellulose,<sup>3</sup> this three-step toluene/ethanol acidic  $\text{NaClO}_2$ –KOH process has shown to isolate 5.3% waxes and organic extracts, 36%

celluloses, 9.5% lignin/hemicelluloses, and 14% silica from rice straw, that is, 65% of rice straw. The lignin/hemicelluloses and silica were eventually converted to 1.3% AC and 14% pure silica.

**Surface and Morphology of Activated Carbon and Silica.** The LH powders were gray in color and appeared as packed particulates in over 20  $\mu\text{m}$  sizes (Figure 5a). After pyrolysis at 800  $^\circ\text{C}$  for 30 min, the obtained AC appeared as irregularly shaped porous clusters of 100–500 nm-sized

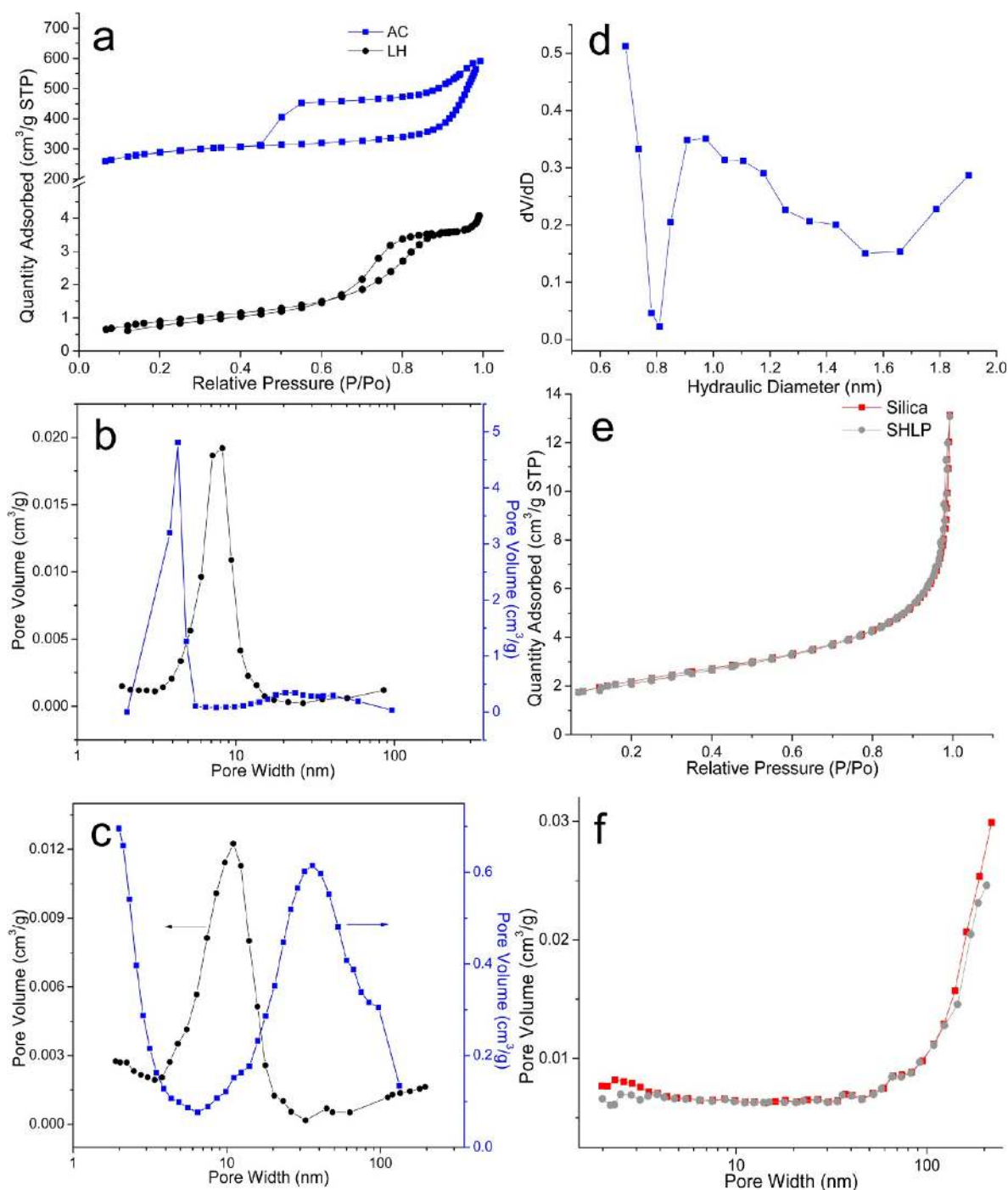


**Figure 6.** Nitrogen adsorption–desorption isotherms of (a,b,c,d) of LH and AC (800 °C, 0.5 h, N<sub>2</sub>) and (e,f) SHLP and silica (500 °C, 0.5 h, air): (a,e) isotherm, (b) BJH neck-size distribution, (c,f) BJH pore/cavity width distribution, and (d) micropore hydraulic diameter distribution.

442 particles (Figure 5b), which are much smaller than the ACs in  
 443 the previous studies.<sup>16–18</sup> These much shorter diffusion lengths  
 444 contribute to faster adsorption rate, which is a desirable  
 445 property of AC adsorbent. The TEM images showed the semi-  
 446 crescent AC particles had about a 450 nm Feret diameter. The  
 447 randomly distributed slit-shaped micropores and small  
 448 mesopores were observed within the particle (Figure 5c).  
 449 Such porosity was generated by sodium carbonate activation as  
 450 well as pyrolytic decomposition of hemicelluloses and removal  
 451 of sodium byproducts from washing.  
 452 The SEM showed smaller and more narrowly distributed  
 453 SHLP particles with increasing PEO concentrations (Figure S2,

Supporting Information). Semi-spherical particles from 100 to 454  
 200 nm sizes were obtained at 0.2% PEO. With increasing PEO 455  
 concentrations to 0.35%, more uniformly sized nanospheres 456  
 between 100 and 150 nm were formed (Figure 5d–f), possibly 457  
 due to better capping of particles preventing them from 458  
 aggregating and/or growing into larger particles. At 0.5 wt % 459  
 PEO and above, however, the particles became irregularly 460  
 shaped and polydispersed in sizes less than 50 nm, possibly 461  
 from easy sintering during calcination. Only the SLHP particles 462  
 precipitated from 0.35% acidified PEO remained similar in size 463  
 after calcinations. Such a PEO precipitation approach has 464  
 proven to be fast and effective, without the need for the time- 465



Table 2. Physical Properties of LH, AC, SHLP, and Silica Deduced from N<sub>2</sub> Adsorption–Desorption at 77 K

	BET surface area (m <sup>2</sup> /g)	BJH adsorption cumulative surface area between 1.7 and 300 nm width (m <sup>2</sup> /g)	single-point desorption pore volume (cm <sup>3</sup> /g)	BJH adsorption cumulative volume of pore between 1.7 and 300 nm (cm <sup>3</sup> /g)	<i>t</i> -plot-derived micropore surface area between 0.7 and 2 nm width (m <sup>2</sup> /g)	<i>t</i> -plot-derived micropore volume (cm <sup>3</sup> /g)
LH	3	3	0.006	0.006	0	0
AC	997	249	0.90	0.58	592	0.27
SHLP	7.9	6.6	0.015	0.020	0	0
silica	7.2	6.1	0.014	0.019	0	0

466 consuming aging process. The obtained silica spheres were  
 467 much more uniform in both size and shape than those  
 468 previously reported.<sup>17,20</sup> The high size uniformity is crucial to  
 469 fine-tune the properties of silica particles to be used as additive/  
 470 fillers for composites or further functionalized for other  
 471 applications.

472 **Porous Structure of Activated Carbon and Silica.** The  
 473 as-prepared LH powders appeared flaky and showed a H2  
 474 hysteresis in a BET nitrogen adsorption isotherm (Figure 6a)  
 475 with a very low surface area of 3 m<sup>2</sup>/g and a pore volume of  
 476 0.006 cm<sup>3</sup>/g, indicative of their nonporous nature (Table 2).  
 477 The extremely low surface area was attributed to secondary  
 478 porosity, for example, interparticulate mesopores distributed  
 479 between 3 and 30 nm, and peaked at 10 nm as shown in the  
 480 pore width distribution (Figure 6b). Carbonization at 800 °C  
 481 for 30 min significantly increased the BET surface area of the  
 482 submicrometer-sized AC particles to 997 m<sup>2</sup>/g and total pore  
 483 volume to 0.9 cm<sup>3</sup>/g, that is, a specific surface area over 330  
 484 times of that of the LH precursor. The BJH surface area and  
 485 pore volume of the meso/macropores between 1.7 and 300 nm  
 486 were estimated to be 249 m<sup>2</sup>/g and 0.58 cm<sup>3</sup>/g, respectively,  
 487 and those of the *t*-plot-derived micropores below 2 nm were  
 488 approximated to be 592 m<sup>2</sup>/g and 0.27 cm<sup>3</sup>/g, respectively  
 489 (Table 2) Therefore, the surface area was mostly attributed to  
 490 the micropores, while the pore volume was attributed to the  
 491 larger mesopores and macropores. The type IV isotherm with  
 492 noticeable H4 hysteresis observed on AC (Figure 6a) suggests a  
 493 slit-like micro/mesoporous structure.<sup>35</sup> The micropores ranged  
 494 from 0.8 to 1.6 nm in diameter, peaking at 0.95 nm (Figure 6d),  
 495 whereas the mesopores were bimodally distributed between 2  
 496 and 6 nm as well as between 10 nm to submicrometer (Figure  
 497 6c), consistent with TEM observations (Figure 5c). The  
 498 adsorption–desorption isotherms exhibited characteristic step-  
 499 down at 0.45 *P*/*P*<sub>0</sub>, while the pore width distribution derived  
 500 from the desorption branch showed a distinct peak around 4  
 501 nm from cavitation of nitrogen during desorption (Figure 6b),  
 502 indicating mesopores connected by slit-like micropores  
 503 consistent to similar observations by others.<sup>36,37</sup> The internal  
 504 micropores and mesopores contributed mostly to the high  
 505 surface area and pore volume of AC, while the large  
 506 macropores likely from interparticle spacing (secondary  
 507 porosity) as shown in the SEM (Figure 5b) contributed little.

508 Both SHLP and silica exhibited type II BET nitrogen  
 509 adsorption isotherms, typical of nonporous and macroporous  
 510 materials with weak affinities to nitrogen (Figure 6e). Both had  
 511 very similarly low BET surface area and pore volume of about 7  
 512 m<sup>2</sup>/g and 0.015 cm<sup>3</sup>/g, respectively, as well as BJH mesoporous  
 513 surface area and pore volume of about 6 m<sup>2</sup>/g and 0.002 cm<sup>3</sup>/g,  
 514 respectively (Table 2). Only macropores larger than 100 nm  
 515 were observed in both (Figure 6f). There was no evidence of  
 516 mesopores. These observations were consistent with their low  
 517 surface areas and pore volume that were mainly attributed to  
 518 the external particle surfaces and interparticulate spacing. In  
 519 calcination of SHLP, the organic hemicelluloses, lignin, and

PEO components were removed, leaving only silica with no  
 520 porosity as indicated by the nitrogen adsorption–desorption  
 521 analysis. This nonporous structure suggests that the organic  
 522 components are either mainly capped on the silica particle  
 523 surface and/or well mixed with silica to create micropores that  
 524 collapse during calcinations or are below the 0.3 nm nitrogen  
 525 adsorption–detection level of the instrument used. 526

## 527 CONCLUSION

528 This study has demonstrated the feasibility to optimally isolate  
 529 the lignin, hemicellulose, and silica components from rice straw,  
 530 along cellulose previously reported,<sup>3</sup> and efficiently convert  
 531 them into advanced materials. An efficient three-step toluene/  
 532 ethanol, NaClO<sub>2</sub>, and KOH isolation process has been  
 533 successfully devised for isolating two-thirds of crude rice  
 534 straw into at least 36% pure cellulose from rice straw while  
 535 generating two filtrates, 2.8% lignin-rich LH and 20.7% silica–  
 536 hemicellulose-rich SHL as precursors for activated carbon and  
 537 silica particles, respectively. The NaClO<sub>2</sub> dissolution stream  
 538 from the dewaxed rice straw contains oxidized lignin and  
 539 hemicelluloses as carbon precursors as well as sodium  
 540 carbonates as activating chemicals that can be precipitated for  
 541 direct carbonization at 800 °C to yield 1.3% activated carbon  
 542 particles with submicrometer sizes between 100 and 500 nm as  
 543 well as high specific surface area (997 m<sup>2</sup>/g) and pore volume  
 544 (0.90 cm<sup>3</sup>/g). The KOH dissolution stream from NaClO<sub>2</sub>-  
 545 treated rice straw contains mainly potassium silicate and a small  
 546 amount of lignin/hemicelluloses and could be precipitated by  
 547 dilute (0.35%) acidified poly(ethylene oxide) and calcinated to  
 548 yield 14% pure, nonporous, silica nanospheres in 100 to 120  
 549 nm diameters. This is the first report of highly efficient  
 550 processes that optimally isolated and fully utilized all major rice  
 551 straw components, the highest quantity agricultural crop  
 552 byproduct in the world. Together with nanocellulose products  
 553 reported,<sup>3</sup> 80% of the isolated components or 51.5% of crude  
 554 rice straw was converted into high quality particulates of highly  
 555 porous activated carbon particles and uniformly sized non-  
 556 porous silica nanoparticles. These high quality nanomaterials  
 557 can provide broadly available feedstock for advanced materials.

## 558 ASSOCIATED CONTENT

### 559 Supporting Information

560 EDX of LH after calcination and SEMs of silica particles  
 561 precipitated by acidified PEO of different concentrations before  
 562 and after calcination. This material is available free of charge via  
 563 the Internet at <http://pubs.acs.org>.

## 564 AUTHOR INFORMATION

### 565 Corresponding Author

566 \*E-mail: ylhsieh@ucdavis.edu.

### 567 Notes

568 The authors declare no competing financial interest.

## 569 ■ ACKNOWLEDGMENTS

570 The authors appreciate the support of the California Rice  
571 Research Board (Project RU-9).

## 572 ■ REFERENCES

- 573 (1) Alonso, D. M.; Bond, J. Q.; Dumesic, J. A. Catalytic conversion of  
574 biomass to biofuels. *Green Chem.* **2010**, *12* (9), 1493–1513.
- 575 (2) Stocker, M. Biofuels and biomass-to-liquid fuels in the  
576 biorefinery: Catalytic conversion of lignocellulosic biomass using  
577 porous materials. *Angew. Chem., Int. Ed.* **2008**, *47* (48), 9200–9211.
- 578 (3) Wyman, C. E. Ethanol from lignocellulosic biomass –  
579 Technology, economics, and opportunities. *Bioresour. Technol.* **1994**,  
580 *50* (1), 3–16.
- 581 (4) Maschio, G.; Koufopoulos, C.; Lucchesi, A. Pyrolysis, a promising  
582 route for biomass utilization. *Bioresour. Technol.* **1992**, *42* (3), 219–  
583 231.
- 584 (5) Datar, R.; Huang, J.; Maness, P. C.; Mohagheghi, A.; Czernik, S.;  
585 Chornet, E. Hydrogen production from the fermentation of corn  
586 stover biomass pretreated with a steam-explosion process. *Int. J.*  
587 *Hydrogen Energy* **2007**, *32* (8), 932–939.
- 588 (6) Lu, P.; Hsieh, Y. L. Preparation and characterization of cellulose  
589 nanocrystals from rice straw. *Carbohydr. Polym.* **2012**, *87* (1), 564–  
590 573.
- 591 (7) Alemdar, A.; Sain, M. Isolation and characterization of nanofibers  
592 from agricultural residues – Wheat straw and soy hulls. *Bioresour.*  
593 *Technol.* **2008**, *99* (6), 1664–1671.
- 594 (8) Tay, T.; Ucar, S.; Karagoz, S. Preparation and characterization of  
595 activated carbon from waste biomass. *J. Hazard. Mater.* **2009**, *165* (1–  
596 3), 481–485.
- 597 (9) Dodson, J. R.; Cooper, E. C.; Hunt, A. J.; Matharu, A.; Cole, J.;  
598 Minihan, A.; Clark, J. H.; Macquarrie, D. J. Alkali silicates and  
599 structured mesoporous silicas from biomass power station wastes: The  
600 emergence of bio-MCMs. *Green Chem.* **2013**, *15* (5), 1203–1210.
- 601 (10) Mansour, N. A. L.; Hanna, S. B. Silicon-carbide and nitride from  
602 rice hulls 0.2. Effect of iron on the formation of silicon-carbide. *Trans.*  
603 *J. Br. Ceram. Soc.* **1979**, *78* (6), 132–136.
- 604 (11) FAOSTAT, 2011. Food and Agriculture Organization of the  
605 United Nations. <http://faostat.fao.org/>.
- 606 (12) Moo-Young, M., Ed.; *Comprehensive Biotechnology: The*  
607 *Principles, Applications, and Regulations of Biotechnology in Industry,*  
608 *Agriculture, and Medicine*; Pergamon Press: Oxford, U.K., 1985.
- 609 (13) Binod, P.; Sindhu, R.; Singhanian, R. R.; Vikram, S.; Devi, L.;  
610 Nagalakshmi, S.; Kurien, N.; Sukumaran, R. K.; Pandey, A. Bioethanol  
611 production from rice straw: An overview. *Bioresour. Technol.* **2010**, *101*  
612 (13), 4767–4774.
- 613 (14) Huang, Y. F.; Kuan, W. H.; Lo, S. L.; Lin, C. F. Hydrogen-rich  
614 fuel gas from rice straw via microwave-induced pyrolysis. *Bioresour.*  
615 *Technol.* **2010**, *101* (6), 1968–1973.
- 616 (15) Reddy, N.; Yang, Y. Q. Properties of high-quality long natural  
617 cellulose fibers from rice straw. *J. Agric. Food Chem.* **2006**, *54* (21),  
618 8077–8081.
- 619 (16) Basta, A. H.; Fierro, V.; Ei-Saied, H.; Celzard, A. 2-Step KOH  
620 activation of rice straw: An efficient method for preparing high-  
621 performance activated carbons. *Bioresour. Technol.* **2009**, *100* (17),  
622 3941–3947.
- 623 (17) An, D. M.; Guo, Y. P.; Zou, B.; Zhu, Y. C.; Wang, Z. C. A study  
624 on the consecutive preparation of silica powders and active carbon  
625 from rice husk ash. *Biomass Bioenergy* **2011**, *35* (3), 1227–1234.
- 626 (18) Gao, P.; Liu, Z. H.; Xue, G.; Han, B.; Zhou, M. H. Preparation  
627 and characterization of activated carbon produced from rice straw by  
628 (NH<sub>4</sub>)<sub>2</sub>HPO<sub>4</sub> activation. *Bioresour. Technol.* **2011**, *102* (3), 3645–  
629 3648.
- 630 (19) Zaky, R. R.; Hessien, M. M.; El-Midany, A. A.; Khedr, M. H.;  
631 Abdel-Aal, E. A.; El-Barawy, K. A. Preparation of silica nanoparticles  
632 from semi-burned rice straw ash. *Powder Technol.* **2008**, *185* (1), 31–  
633 35.
- 634 (20) Hessien, M. M.; Rashad, M. M.; Zaky, R. R.; Abdel-Aal, E. A.;  
635 El-Barawy, K. A. Controlling the synthesis conditions for silica

- nanosphere from semi-burned rice straw. *Mater. Sci. Eng., B* **2009**, *162* *636*  
637 (1), 14–21.
- (21) Lu, P.; Hsieh, Y. L. Highly pure amorphous silica nano-disks *638*  
639 from rice straw. *Powder Technol.* **2012**, *225*, 149–155.
- (22) Patel, M.; Kumari, P. Silicon-carbide from sugarcane leaf and *640*  
641 rice straw. *J. Mater. Sci. Lett.* **1990**, *9* (4), 375–376.
- (23) Kadam, K. L.; Forrest, L. H.; Jacobson, W. A. Rice straw as a *642*  
643 lignocellulosic resource: Collection, processing, transportation, and  
644 environmental aspects. *Biomass Bioenergy* **2000**, *18* (5), 369–389.
- (24) Xiao, B.; Sun, X. F.; Sun, R. C. Chemical, structural, and thermal *645*  
646 characterizations of alkali-soluble lignins and hemicelluloses, and  
647 cellulose from maize stems, rye straw, and rice straw. *Polym. Degrad.*  
648 *Stab.* **2001**, *74* (2), 307–319.
- (25) Sangnark, A.; Noomhorm, A. Chemical, physical and baking *649*  
650 properties of dietary fiber prepared from rice straw. *Food Res. Int.*  
651 **2004**, *37* (1), 66–74.
- (26) Karimi, K.; Emtiazi, G.; Taherzadeh, M. J. Production of ethanol *652*  
653 and mycelial biomass from rice straw hemicellulose hydrolyzate by  
654 *Mucor indicus*. *Process Biochem.* **2006**, *41* (3), 653–658.
- (27) Kargbo, F. R.; King, J. J.; Zhang, Y. L. Pretreatment for energy *655*  
656 use of rice straw: A review. *Afr. J. Agric. Res.* **2009**, *4* (13), 1560–1565.
- (28) Jiang, F.; Hsieh, Y. L. Chemically and mechanically isolated *657*  
658 nanocellulose and their self-assembled structures. *Carbohydr. Polym.*  
659 **2013**, *95* (1), 32–40.
- (29) Mikhail, R. S.; Brunauer, S.; Bodor, E. E. Investigations of a *660*  
661 complete pore structure analysis. I. Analysis of micropores. *J. Colloid*  
662 *Interface Sci.* **1968**, *26* (1), 45–8.
- (30) Harkins, W. D.; Jura, G. An adsorption method for the *663*  
664 determination of the area of a solid without the assumption of a  
665 molecular area, and the area occupied by nitrogen molecules on the  
666 surfaces of solids. *J. Chem. Phys.* **1943**, *11* (9), 431–432.
- (31) He, L. F.; Terashima, N. Formation and structure of lignin *667*  
668 in monocotyledons 0.4. Deposition process and structural diversity of the  
669 lignin in the cell-wall of sugarcane and rice plant studied by ultraviolet  
670 microscopic spectroscopy. *Holzforchung* **1991**, *45* (3), 191–198.
- (32) Sun, R. C.; Tomkinson, J.; Mao, F. C.; Sun, X. F. *671*  
672 Physicochemical characterization of lignins from rice straw by  
673 hydrogen peroxide treatment. *J. Appl. Polym. Sci.* **2001**, *79* (4),  
674 719–732.
- (33) Brauns, F. E. *The Chemistry of Lignin*; Academic Press: New *675*  
676 York, 1952.
- (34) Bikova, T.; Treimanis, A. UV-absorbance of oxidized xylan and *677*  
678 monocarboxyl cellulose in alkaline solutions. *Carbohydr. Polym.* **2004**,  
679 *55* (3), 315–322.
- (35) Seaton, N.; Reinoso, F. R.; Llewellyn, P.; Kaskel, S., Eds.; *680*  
681 *Characterisation of Porous Solids VIII. Proceedings of the 8th International*  
682 *Symposium on the Characterisation of Porous Solids*; RSC Publishing:  
683 London, 2009.
- (36) Ravikovitch, P. I.; Neimark, A. V. Experimental confirmation of *684*  
685 different mechanisms of evaporation from ink-bottle type pores:  
686 Equilibrium, pore blocking, and cavitation. *Langmuir* **2002**, *18* (25),  
687 9830–9837.
- (37) Thommes, M.; Smarsly, B.; Groenewolt, M.; Ravikovitch, P. I.; *688*  
689 Neimark, A. V. Adsorption hysteresis of nitrogen and argon in pore  
690 networks and characterization of novel micro- and mesoporous silicas.  
691 *Langmuir* **2006**, *22* (2), 756–764.